Self-referenced sensor utilizing extra-ordinary optical transmission from metal nanoslits array

Sachin Kumar Srivastava[1,2,*] and Ibrahim Abdulhalim[1,2,3,4]

[1]*Department of Electro-optic Engineering, Ben Gurion University of the Negev, Beer Sheva 84105, Israel*

[2]*Ilse Katz Institute for Nanoscale Science and Technology, Ben Gurion University of the Negev, Beer Sheva 84105, Israel*

[3]*School of Materials Science and Engineering, Nanyang Technological University, 637722, Singapore*

[4]*e-mail: abdulhlm@bgu.ac.il*

**Corresponding author: sachinchitransh@gmail.com*

Received March 11, 2015; revised April 27, 2015; accepted April 28, 2015;
posted April 30, 2015 (Doc. ID 235893); published May 15, 2015

We report the first self-referenced sensor based on the extraordinary optical transmission (EOT) of metal-nanoslits array in the near-infra-red (NIR) telecommunication window of the electromagnetic spectrum. The nanoslits array shows two enhanced transmission peaks, out of which one shows a red shift with an increase in the refractive index of the analyte medium, while the other remains fixed. We demonstrate the detection of small amounts of water in ethanol using the nanoslits array chip. The present study might be useful in developing ultra-small biosensor chips integrated to optical fibers for online monitoring and remote sensing applications. © 2015 Optical Society of America

OCIS codes: (050.6624) Subwavelength structures; (050.5745) Resonance domain; (130.3060) Infrared; (130.6010) Sensors.

http://dx.doi.org/10.1364/OL.40.002425

Extraordinary optical transmission (EOT) is the phenomenon of the enhancement of the transmission from sub wavelength apertures in nano-metallic films [1,2]. When the apertures are periodic such as nanoslits array, the enhancement in the transmission is attributed to the interaction between the incident radiation and various modes of in-plane surface plasmons (SPs) supported by the periodic structure. However, Fabry–Perot-like behavior from such structures was also observed, where the EOT was attributed to the resonant cavity-enhanced transmission [3]. Despite multiple explanations, a control experiment from Ebbsen *et al.* strongly supported that EOT is a result of plasmons as no enhancement was observed in a similar structure with nonplasmonic materials [1]. Earlier reports from our group and others demonstrated that dual-surface plasmon modes can be excited in metallic nanoslits arrays [4–6]. However, resonance wavelengths corresponding to both the SP modes changed with the change in the refractive indices of the superstrate medium [5]. Such nanoslits arrays were utilized for sensing applications in water environment by considering the shift in resonance wavelength of one of the extraordinarily enhanced transmitted optical peaks [5]. The shift in resonance peaks were attributed to surface plasmons and cavity modes. The phenomenon of EOT has been used for sensing by many others, because the surface plasmon-assisted transmission gives high sensitivity [7,8]. The sensitivity is linear with the resonance wavelength, and therefore, there is a great benefit in working in the infrared, particularly at wavelengths in the telecommunication window where sources, fibers, and detectors are available off the shelf. This was proved in our earlier work [9]; however, the substrate used in that work was BK7, which caused the reference peak to exist at longer wavelengths that could not be observed. In the present Letter, we demonstrate the self-referenced sensing on a nanometallic slits array, both via simulations and experiments and confirm that both the EOT peaks are due to the plasmonic modes at the interfaces, one corresponding to the metal slit–analyte interface and another to the metal slit–substrate interface. Further, the self-referenced mechanism was supported by studying the field profiles in the analyte medium at the two resonances. A schematic of the designed nanoslits array is shown in Fig. 1(a), while Fig. 1(b) shows the SEM images of the nanoslits array fabricated by e-beam lithography. The gold (Au) nanoslits array of 22-nm height and 70-nm groove width with a period of 1120 nm was designed. A cover layer of 20 nm of SiO_2 was added to protect the Au nanoslits array from degradation. The dimensions of the nanoslits array were optimized for maximum performance and operation in the NIR communication window. This spectral range was considered because of easy access of commercially available light sources and detectors, which can be integrated with optical fibers for online monitoring and remote sensing applications. Such a method may be quite useful in brain sensing or invasive online monitoring of blood analytes by placing the fiber integrated nanoslits array sensor in catheters.

The simulated transmitted spectra, obtained by using scattering matrix propagation analysis [10], at normal incidence on the nanoslits array for varying refractive indices of the analyte medium have been plotted in

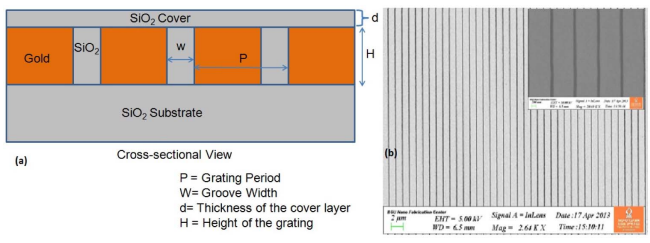

Fig. 1. (a) Illustration of the cross-section of the nanoslits array; (b) SEM images of the fabricated nanoslits array.

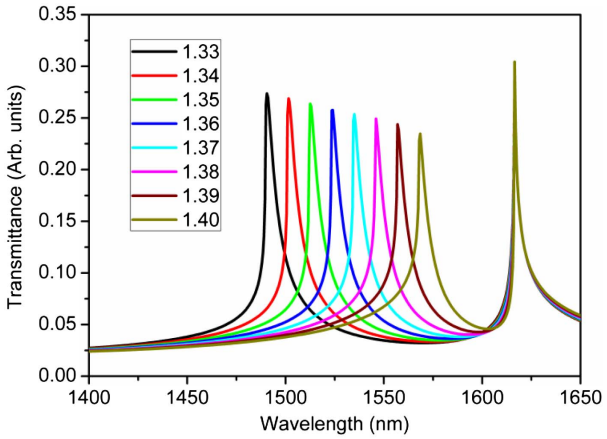

Fig. 2. Simulated transmission spectra for varying refractive indices.

Fig. 2. It is observed that for each value of the analyte refractive index, two enhanced transmission peaks are observed. An increase in the refractive index of the analyte medium leads to a red-shift in the transmission peak at smaller wavelengths (λ_1), while the transmission peak at the larger wavelength (λ_2) remains unaffected. To understand the optical response of the nanostructure, we have simulated the transmission spectra by varying the refractive index of the substrate (MgF_2 and SiO_2) while keeping that of the analyte (H_2O) constant. In Fig. 3, it is observed that the λ_1 peak remains fixed, while the λ_2 peak varies for MgF_2 and SiO_2 substrates. From Figs. 2 and 3, it is obvious that the λ_1 peak responds to the refractive index variations at the analyte–nanoslits interface, while λ_2 responds to that on the nanoslits–substrate interface. Hence, the response obtained in Fig. 2 can be used for self-referenced sensing applications. The two transmission peaks may be attributed to quantized surface plasmons, if considered as metamaterials [11–13]. However, the origin of two such modes can simply be predicated by Eq. (1) [4]:

$$\lambda_{ij} = \frac{P}{i}\mathrm{Re}\left[\sqrt{\frac{\varepsilon_m\varepsilon_j}{\varepsilon_m+\varepsilon_j}}\right] \quad \begin{cases} i = 1, 2, \ldots \\ j = 1, 2 \end{cases}, \qquad (1)$$

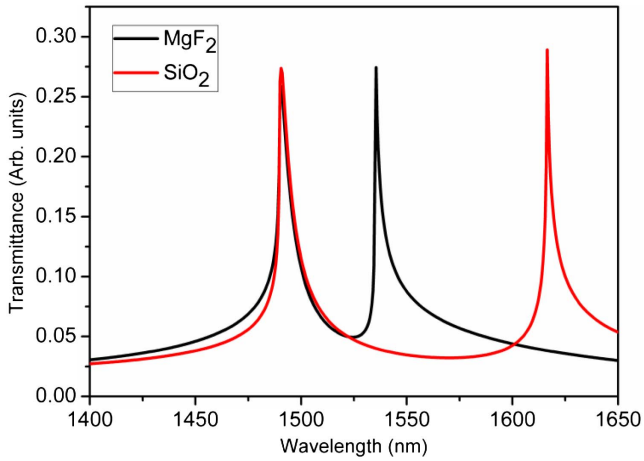

Fig. 3. Simulated transmission spectra for different substrates.

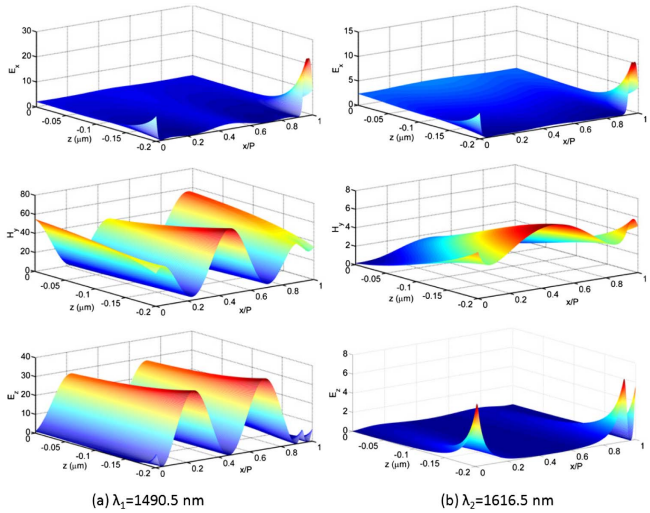

Fig. 4. TM component field profiles in the analyte medium (water) for both resonances of the nanoslits array.

where, i denotes the diffraction order, ε_m represents the dielectric function of the metal and ε_j the dielectric constants of analyte or substrate for $j = 1$ or 2, respectively. Eq. (1) has been well confirmed both theoretically and experimentally [4,5,8,14]. According to Eq. (1), the transmission peak at smaller wavelength (λ_1) corresponds to the SP mode at the nanoslits–analyte interface, while that at the larger wavelength (λ_2) can be attributed to the SP mode at the nanoslits–substrate interface. Further, in Fig. 4 we have plotted the components of the TM polarized field in the analyte for both the resonance wavelengths at normal incidence to learn the effect of both the SP fields in the analyte region. It can be seen from the figure that the field at λ_1 is more than ten times larger in magnitude than that at λ_2. Also, the H_y and E_z field components at λ_2 decay quite rapidly as compared to that of λ_1. Also, the field is mostly confined in the grooves only and not throughout the surface. Hence, eventually almost "no" field at λ_2 is seen by the analyte medium making the transmission peak unaffected due to the changes in analyte refractive index. The penetration depth in gold due to SPR for the gold–SiO_2 interface at 1616.5 nm is about 25 nm, which further supports the fact that the λ_2 resonance is not affected by the variations in the analyte refractive index. Further, sample solutions of water in ethanol with varying percentages ranging from 0% to 100% were prepared, and transmission spectra were recorded for a uniform film of 77-μm thickness of the analyte medium, which was prepared with the help of a spacer of the same thickness over the nanoslits array. Ethanol is found to be a potential alternative to conventional fuel and is regularly used in medical industry and where it is required in its purest forms. For instance, ethanol must be at least 94% pure for its use as a bio-fuel, while in medicine, it must be 100% pure. Water comes as an intrinsic impurity in ethanol when it is manufactured from molasses [15]. Hence, detection of small water percentages in ethanol is an important problem. The schematic of the transmission setup is shown in Fig. 5. Light from a polychromatic source connected to an optical fiber was collimated with the help of an achromatic

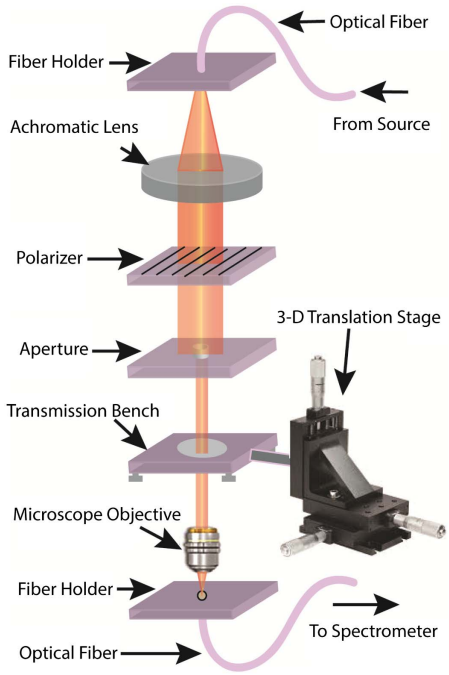

Fig. 5. Schematic of the EOT experimental setup.

lens and passed through a polarizer. Further, an aperture was used to limit the dimensions of the beam to that of the nanoslits array. A tilt stage with 3D-translation mechanism aligns the nanoslits array to the incident beam at normal incidence. Further, the light transmitted off the nanoslits array was focused with a microscope objective on the tip of a fiber connected to a spectrometer.

The recorded transmission spectra for varying percentages of water in ethanol have been plotted in Fig. 6. It is observed that similar to the simulated curves, two transmission peaks are observed for each sample solution. Also, with an increase in water percentage, a shift in first-resonance wavelength is observed, the second-resonance peak being constant. The experimental transmission spectra do not exactly match with the simulated ones due to tolerance in various parameters during fabrication of the nanoslits array. However, more importantly, similar kind of response is achieved. To assess

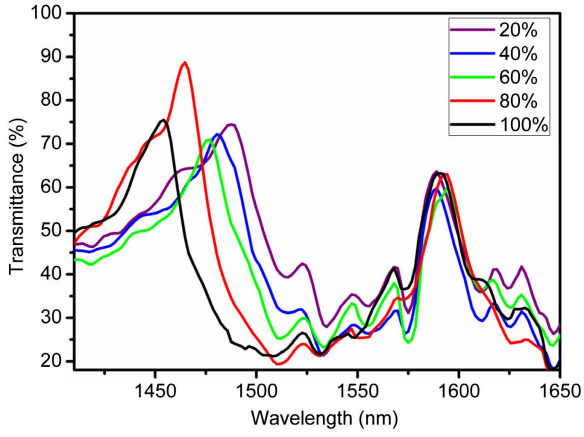

Fig. 6. Experimental transmission spectra for varying concentrations of water in ethanol.

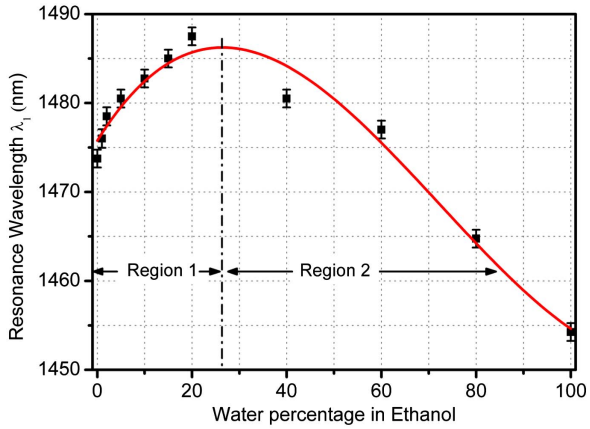

Fig. 7. Variation of first resonance with water percentage in ethanol.

more precise quantitative response of the nanoslits array, we have plotted the variation of the first resonance wavelength with an increase in percentage of water in ethanol in Fig. 7. It is observed that the resonance wavelength corresponding to pure water is 1454 nm, while that for pure ethanol is 1474 nm, which is qualitatively justified according to the simulations, as the refractive index of water is 1.33, while that of ethanol is 1.36. However, with an increase in water percentage in ethanol, a red shift in resonance wavelength is observed, which suggests that the refractive index of the water–ethanol mixture increases until about 20% concentration of water in ethanol. This is contrary to normal belief that the refractive index of a mixture of two completely permissible liquids must lie in between the refractive indices of them. This kind of discrepancy was resolved by measuring the refractive indices of such mixtures with different water proportions. The slight increase in the refractive index of the water–ethanol mixtures at small water percentages was attributed to the formation of ethanol–water clusters due to hydrogen bonding, which lead to slight increase in density and hence the refractive index [16]. After about 22% concentration of water in ethanol, the clusters of ethanol–water make homogenous mixture, which leads to disappearance of the clusters and hence the refractive index decreases. However, this kind of response curve cannot predict the accurate water percentage in ethanol for the whole range, as for certain values the same resonance wavelength corresponds to two water percentages. For example, the resonance wavelengths for 0.5% and 60% water percentages are almost the same. Since ethanol needs to be used in its purest forms, region 1 of Fig. 7 is more useful and can be used for sensing of small water percentages in ethanol. Hence, this sensor can be used for detection of small water percentages in ethanol. We have plotted the response curve for small water percentages in Fig. 8. It is almost linear for small water concentrations. The sensitivity of the sensor calculated from this curve is 0.69 nm/water %. The error bars were calculated by considering the resolution of the spectrometer and that of the pipette used for making sample solutions.

In conclusion, we have demonstrated, both by simulations and experiments, a self-referenced EOT-based

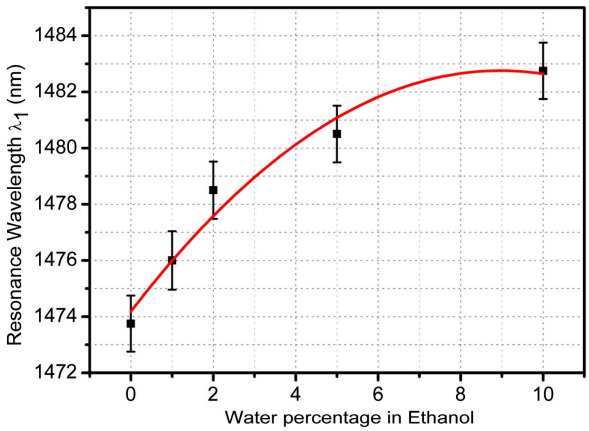

Fig. 8. Variation of first resonance wavelength with small water percentages in ethanol.

sensor for the detection of small percentages of water in ethanol using a nanoslits array of Au. The sensor may further be utilized for the detection of blood analytes, as it can predict the variations very accurately due to self referencing.

This research is partially supported by the National Research Foundation, Prime Minister's Office, Singapore and Ben-Gurion University of the Negev, Israel. Sachin thanks to the Council for Higher Education of the State of Israel for PBC postdoctoral fellowship. The help with the computer implementation by Prof. M. Auslender and Ph.D. student M. Zohar is acknowledged.

References

1. T. W. Ebbesen, H. J. Lezec, H. F. Ghaemi, T. Thio, and P. A. Wolff, Nature **391**, 667 (1998).
2. I. Avrutsky, Y. Zhao, and V. Kochergin, Opt. Lett. **25**, 595 (2000).
3. A. T. M. Anishur Rahman, P. Majewski, and K. Vasilev, Opt. Lett. **37**, 1742 (2012).
4. A. Karabchevsky, M. Auslender, and I. Abdulhalim, J. Nanophoton. **5**, 051821 (2011).
5. A. Karabchevsky, O. Krasnykov, M. Auslender, B. Hadad, A. Goldner, and I. Abdulhalim, Plasmonics **4**, 281 (2009).
6. S. M. Orbons, M. I. Haftel, C. Schlockermann, D. Freeman, M. Milicevic, T. J. Davis, B. Luther-Davies, D. N. Jamieson, and A. Roberts, Opt. Lett. **33**, 821 (2008).
7. W. Yue, Z. Wang, Y. Yang, J. Li, Y. Wu, L. Chen, B. Ooi, X. Wang, and X.-x. Zhang, Nanoscale **6**, 7917 (2014).
8. K.-L. Lee, J.-B. Huang, J.-W. Chang, S.-H. Wu, and P.-K. Wei, Sci. Rep. **5**, 8547 (2015).
9. O. Krasnykov, A. Karabchevsky, A. Shalabney, M. Auslender, and I. Abdulhalim, Opt. Commun. **284**, 1435 (2011).
10. M. Auslender and S. Hava, Opt. Lett. **21**, 1765 (1996).
11. J. D. Cox, M. R. Singh, M. A. Antón, and F. Carreño, J. Phys. Condens. Matter **25**, 385302 (2013).
12. M. R. Singh, J. D. Cox, and M. Brzozowski, J. Phys. D **47**, 085101 (2014).
13. M. R. Singh, M. Brzozowski, and C. Racknor, J. Phys. D **48**, 145301 (2015).
14. E. Popov, M. Nevière, S. Enoch, and R. Reinisch, Phys. Rev. B **62**, 16100 (2000).
15. S. K. Srivastava and B. D. Gupta, Open Opt. J. Bentham **7**, 58 (2013).
16. S. K. Srivastava, R. Verma, and B. D. Gupta, Sens. Actuators B **153**, 194 (2011).